Effect of Stabilization on Creep Crack Growth in High-Density Polyethylene

G. Pinter, R. W. Lang

Institute of Materials Science and Testing of Plastics, Montanuniversität Leoben, Franz-Josef-Straße 18, A-8700 Leoben, Austria

ABSTRACT: Polyolefins, particularly polyethylene, are known to fail via crack initiation and crack propagation when exposed to multiaxial long-term static stresses at elevated temperatures. Using concepts of linear elastic fracture mechanics, this article describes and discusses the effects of stabilization on the kinetics of creep crack growth (CCG) in high-density polyethylene (PE-HD) and the failure micromechanisms involved. As for the influence of stabilization, six PE-HD formulations (two polymer types, each with three stabilizer systems) were investigated. CCG initiation times and CCG rates were determined at 60 and 80°C in distilled water as functions of the crack tip stress field characterized by the stress intensity factor. Although no influence of the stabilizer type was found in either polymer type for CCG initiation times and CCG rates at high crack speeds, significant effects of the added stabilizer type and concentration were detected for low CCG rates. The observed phenomena were explained in terms of local aging processes in the immediate vicinity of the crack tip, which were controlled by the presence and content of various stabilizers. © 2003 Wiley Periodicals, Inc. J Appl Polym Sci 90: 3191–3207, 2003

Key words: polyethylene (PE); creep; growth; stabilization; ageing

INTRODUCTION

High-density polyethylene (PE-HD) is increasingly used in long-term structural applications (e.g., gas and water pipes, geo membranes, and other mechanically, thermally, and chemically loaded components). With respect to the time-dependent failure behavior, ductile failure is generally observed at high stress levels and short failure times, whereas quasibrittle failure frequently occurs at lower stress levels and correspondingly longer failure times. This phenomenon of quasibrittle, long-term failure of nominally ductile PE-HD under static loads has been investigated over the last 2 decades by numerous authors with fracture mechanics methods.[1–6] With these methods, the kinetics of creep crack growth (CCG) are characterized in terms of the dependence of CCG rates on the applied stress intensity factor (K_I) level.

In recent years, considerable attention has been paid to the effects of various material parameters on the CCG behavior of PE-HD. For example, it has been shown by several investigators[6–9] that CCG rates significantly depend on the average molecular mass and molecular mass distribution, the concentration and length of short-chain branches, and the crystalline morphology [degree of crystallinity (X_c) and lamellar dimensions]. However, no detailed study exists on the influence of stabilization on CCG kinetics. This is somewhat surprising, as it is well known that the stabilizer type and concentration may significantly affect the lifetime of pressurized pipes in the quasibrittle and brittle failure regime.[10,11]

Most recently, the concept of local crack tip aging has been proposed to explain the first experimental findings of stabilizer effects on CCG rates in PE-HD.[6,12,13] The main objective of this article is to study and to describe the effects of different stabilizer systems on the CCG behavior in more detail. For this purpose, two PE-HD types were compounded with three different stabilizer systems, and crack growth experiments under static loads were performed at 60 and 80°C in distilled water. To correlate the experimental findings with molecular and morphological parameters and to explain the results in terms of local failure processes, we extensively characterized the materials before and after the CCG tests were performed.

BACKGROUND

It is generally accepted that the rate of chemical reactions in solid polymers may change significantly under the influence of external or internal stresses.[14] On the one hand, this may be due to substantial changes in the structural and physical parameters of a polymer under the action of mechanical stresses (e.g., molecular conformation, free-volume increases, and changes in the permeability of low-molecular-mass substances).

On the other hand, stress may directly affect the reactivity of deformed macromolecules, thereby altering the effective activation energies for chemical reactions.

The accelerating effects of mechanical stresses on oxidative aging processes were first observed with rubber[15] and designated as mechanical and chemical aging. Popov et al.[14] and Terselius et al.[16] reported the effects of stresses on chemical aging for other polymers, primarily for polyethylene (PE) and polypropylene (PP). In this context, it was pointed out by Costa et al.[17] that although high forces on a molecular level are necessary to mechanically break covalent bonds in polymers, moderate forces may catalyze the scission of bonds when superimposed by chemical reactions. Nevertheless, the most highly loaded bonds will be those also most likely to react.[18,19] As a result, under practical conditions, local aging mechanisms are frequently coactivated by defects or residues of metallic catalysts.[20,21]

A modification of the activation energies of chemical reactions by stresses was originally proposed in a quantitative form by Zhurkov et al.[22] and Bueche.[23] For a stressed polymer, the time to failure is given by an Arrhenius-type expression:

$$\tau = A \exp\left(\frac{\Delta G - B\sigma}{RT}\right) \qquad (1)$$

where ΔG is the energy barrier (activation energy), σ is the applied stress, R is the gas constant, T is the absolute temperature, and A and B (frequently called the activation volume) are constants.

Nevertheless, quantitative estimates of the influence of mechanical stresses on the aging behavior of polymers still encounter many difficulties because of the complexity of the various processes involved.[14,24] Particularly high tensile stresses in the postyield regime have a substantial influence on the molecular orientation and void formation (i.e., crazing) and may thus change the diffusion rates of low molecular substances, thereby altering the reaction rates.[14,25–28] This essentially concerns oxygen molecules, macroradicals, and stabilizers, which are added to polymers to delay aging. In semicrystalline polymers, long-term stresses can also lead to higher X_c values,[14,29–32] and this affects the mobility of oxygen and stabilizer molecules and thus the rate of aging. Interestingly, although it is generally assumed that tensile loads accelerate degradation, compressive loads often delay it.[14,33–36]

Systematic investigations of the effects of stresses and stabilizers on the thermooxidative aging behavior of polymers have been performed so far mainly in long-term tests on pipes internally pressurized at temperatures from 60 to 120°C for time periods of up to 20 years.[11,28,37–39]

These tests have been performed mainly with polyolefins and have been focused on the characterization of global aging phenomena. Nevertheless, it has been recognized by at least some authors that oxidation often originates locally at highly degraded oxidation spots (i.e., the heterogeneous initiation of oxidation).[21,29,40–43] In this initial stage, two processes proceed simultaneously. On the one hand, the degree of oxidation of the regions already involved in oxidation increases, and on the other hand, the reaction front moves by radical diffusion. As pointed out previously, in many situations oxidation initiation occurs at preexisting, randomly distributed areas containing catalytic impurities and can be accelerated by superimposed mechanical stresses.[21]

Moreover, for PP oxidized under tensile stresses, it can be shown that a catastrophic crack always proceeds through highly oxidized zones, whereas the polymeric material away from the fracture zone reveals a much lower degree of oxidation. The oxidation gradient in the fracture zone is strongly dependent on the applied tensile stress.[14]

Hence, although molecular and morphological variations caused by aging processes are accepted as important mechanisms that may affect the long-term failure of polymers,[44,45] very few investigations so far have addressed the potential for enhanced local crack tip aging. As mentioned previously, the hypothesis of local crack tip aging caused by the simultaneous influence of high stresses and thermooxidative environments on the immediate vicinity of a crack tip has been proposed before.[6,12,13,24,46] Corroborating this proposal are investigations on local photooxidative aging in cracked specimens.[47–50]

In the context of the local crack tip aging hypothesis, it should be recalled that the immediate crack tip region in polyolefins and particularly in PE-HD consists of highly stretched fibrils interdispersed by a void network with a high surface-to-volume ratio, which simultaneously is exposed to high stresses beyond yield stress (σ_y) levels and allows for easy access of oxygen. Hence, it may well be expected that stabilization will affect crack tip aging processes, leading to stabilizer-dependent CCG rates in a given polymer.

EXPERIMENTAL

Materials

All investigations in this study were performed with the base polymers (i.e., before compounding and thus without standard additives) of two commercial-grade PE-HD compounds (Borealis AG, Linz, Austria). The material codes for these compounds are PE-HD 1 and PE-HD 2, respectively. The corresponding base polymer codes are PE-HD 1* and PE-HD 2*. Some characteristic material properties of these two commercial PE-HD compounds are summarized in Table I.[51,52]

To study the influence of stabilization on the CCG behavior of PE-HD, we selected two different stabilizer/

TABLE I
Characteristic Properties of Commercial PE-HD Compounds of Which the Corresponding Base Polymers Were Used for Model Formulations for this Study[51,52]

Property	Standard	PE-HD 1	PE-HD 2
M_n (kg/mol)	—	19	16
M_w (kg/mol)	—	80	320
ρ* (g/cm³)	ISO 1183	0.964	0.959
E* (N/mm²)	ISO 527	1600	1450
σ_y* (N/mm²)	ISO 527	32	31

Tested at 23°C and 50% relative humidity.

M_n = number-average molecular mass; M_w = weight average molecular mass; ρ = density.

stabilizer systems. Information on these stabilizer/stabilizer systems along with the stabilizer codes reflecting the concentrations of these stabilizers in the model compounds investigated is provided in Table II. Stabilizer S is a sulfur containing a secondary antioxidant (Santonox R, Monsanto, Brussels, Belgium) and was added at 0.1 mass % to both base polymer types. The stabilizer system K is a mixture of a primary antioxidant and a secondary antioxidant (Irganox B225, Ciba Specialty Chemicals, Inc., Basel, Switzerland) and was added at 0.1 mass % (K1) and 0.2 mass % (K2) to the PE-HD formulations. The stabilizer concentrations chosen were in the range of the usual commercial concentrations used in stabilizing pipes for long-term applications. In addition, the unstabilized base polymer PE-HD 1* was included in the investigations, for which the stabilization code 0 was

defined. Because of the significantly higher mean molecular mass, it was anticipated that pelletizing and compression molding of the unstabilized material PE-HD 2* without significant degradation would not be possible. Hence, no pellets and plaques were produced of this unstabilized material type.

With each of the corresponding two base polymers, three formulations containing different stabilizer systems and stabilizer concentrations (as previously described) were produced. The polymer powder was first mixed with 0.1% calcium stearate to act as a processing lubricant. Then, the various antioxidants were dry-blended in a high-speed mixer and compounded in an extruder (Dolci, Milano, Italy) at 190°C. The extruded material formulations were subsequently pelletized.
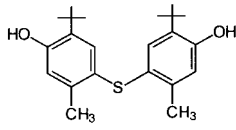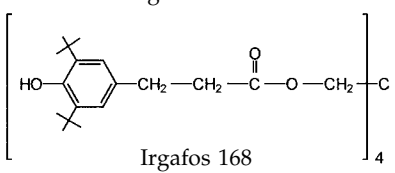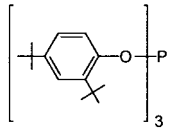
The pellets of the various material formulations were compression-molded into plaques with a nominal thickness of 12 mm at a temperature of 180°C and a pressure of 100 bar (the other plaque dimensions were 190 mm × 190 mm). The molding time was 15 min; a slow-cooling process under pressure was chosen to guarantee a low degree of residual stresses and distortion.

Test methods

Chemical analyses

High-performance liquid chromatography (HPLC) was used to characterize the types and contents of stabilizers in the plaques produced. The analyses were

TABLE II
Designation, Type, Concentration, Structure, and Properties of the Stabilizers Used in this Study

Stabilizer code	Antioxidant (trade name)	Concentration (mass %)	chemical structure	Molecular mass (g/mol)	Melting range (°C)
			Stabilizer structure and properties		
0	unstabilized	—	—	—	—
S	Santonox R	0.1		358	161
K1	Irganox B225 (Irganox 1010/Irgafos 168 in a ratio of 1:1)	0.1	Irganox 1010 Irgafos 168	1178 647	110–125 180–185
K2	Irganox B225	0.2	See K1	See K1	See K1

performed on a Spectra Physics SP 8800 test system equipped with an ultraviolet–visible detector (Spectra 200) and a hyperchrome column (125 × 4.6 mm) filled with Nucleosil. The method was based on a gradient eluent consisting of methanol, ethyl acetate, and water and on using toluene for dissolving PE at 170°C. After the cooling and precipitation of the polymer with methanol, the stabilizer solution was directly injected.

Thermoanalytical analyses

Both X_c and the oxidation temperature (T_{ox}) were determined with a DuPont 910 differential scanning calorimeter (TA Instruments, Alzenau) at a heating rate of 10 K/min in air. The sample weight was approximately 5–10 mg. The values of X_c were calculated with the relationship $X_c = \Delta H_s/\Delta H_c$, where ΔH_s represents the experimental melting peak area and the value of ΔH_c for 100% crystalline PE is assumed to be 293 J/g.[53] T_{ox} was defined as the temperature at the intersection of the extended baseline with the extrapolated slope of the exotherm.

In addition, the oxidation induction time (OIT) was measured under isothermal conditions at 180°C in air with an isothermal long-term differential thermal analysis device designed and built in our laboratory.[38] The samples were quickly inserted into the preheated cells, and no purge gas was used throughout the experiment. The sample weight was also in the range of 5–10 mg. OIT values were obtained by the intersection of the extended baseline with the extrapolated slope of the exotherm signal.

Rheological analyses

For the rheological characterization of the materials, a Rheometrics model II dynamic analyzer (Rheometrics, Piscataway, NJ) with parallel-plate fixtures (diameter = 25 mm, gap = 1.5 mm) was used. To prevent thermooxidative degradation during testing, we performed all tests under a nitrogen atmosphere. The unstabilized material PE-HD 1*/0 was specifically stabilized with butylhydroxytoluol before testing to prevent degradation while the test was performed. To obtain information on the molecular material state of specimens in the CCG experiments, all rheological tests were carried out on samples and specimens obtained from compression-molded plaques.

In frequency sweeps (0.1–500 rad/s), the complex viscosity (η^*), the storage modulus (G'), and the loss modulus (G'') were determined in the linear viscoelastic deformation range at a shear deformation of 20%. Test temperatures of 150 and 180°C were selected for the PE-HD 1* and PE-HD 2* formulations, respectively. η^* as a function of the frequency (ω) and the crossover point [G_c; i.e., the intersection of $G'(\omega)$ and $G''(\omega)$ curves] were used to characterize the molecular masses of the materials in terms of potential differences.

As the zero viscosity (η^*_0; i.e., a frequency-independent viscosity value at low frequencies) was proportional to the weight-average molecular mass, variations in the distribution of the molecular mass could be estimated from changes in η^*_0 and from the frequency position at which η^* became frequency-dependent.[54] Moreover, G_c in terms of the coordinates for G' (or G'') and ω gave an indication of variations in both the average molecular mass and molecular mass distribution. Increases and decreases in crossover G' (or G'') values indicated narrower and broader molecular mass distributions, respectively. Similarly, increases and decreases in crossover ω values implied lower and higher average molecular masses, respectively.[55]

Alternatively, stress relaxation experiments (shear modulus relaxation) in the nonlinear viscoelastic deformation range were performed to obtain information on potential differences in the molecular mass distributions of the various formulations of a given base polymer type.[56,57] The tests for PE-HD 1* formulations were performed at 150°C at an initial shear deformation of 200%. Experiments for PE-HD 2* formulations were carried out at 200°C and an initial shear deformation of 100%. The different test parameters used for the two base polymer types in all rheological experiments reflected the differences in their molecular masses and molecular mass distributions.

Small-angle X-ray scattering (SAXS)

The average thickness of the crystalline lamella region (L_c) and of the disordered (amorphous) top layers (L_a) was determined by SAXS with a Kratky compact low-angle camera with an entrance slit width of 20 μm (Anton Paar GmbH, Graz, Austria). Samples 2 mm thick were machined from the plaques. As a primary beam, the Ni-filtered (30 μm) radiation of a tube with a copper anode operating at 50 kV and 45 mA was used. The scattered intensities were measured by a linear position-sensitive detector. After the data were desmeared and corrected (Lorentz correction), the value of the average long period was estimated from the first maximum at the lowest scattering angle by the application of Bragg's law. On the basis of X_c of the material [measured by differential scanning calorimetry (DSC), as previously described], the average lamellar thickness was calculated. The thickness distribution curves were extracted from the SAXS data by the fitting of model curves to the smoothed and corrected SAXS data, a morphological two-phase system being assumed.[58]

Infrared spectroscopy

To identify the existence of carbonyl groups that could be formed during oxidation, we used a spectropho-

tometer (model 1600, PerkinElmer, Überlingen, Germany). The measurements were carried out with approximately 200-μm-thick slices, which were cut from the fracture mechanics test specimens after CCG tests. The transmission spectra were collected at 16 scans and a resolution of 2 cm^{-1}. The individual carbonyl groups formed during oxidation were identified by their specific absorption bands in the spectrum (acid groups at 1705 cm^{-1}, ketone groups at 1715 cm^{-1}, and aldehyde and ester groups in the region of 1735–1740 cm^{-1}). A similar methodology for determining aging processes in polyolefins has frequently been used by other researchers.[59]

Tensile tests

The tensile tests were carried out with a screw-driven universal-tension/compression testing machine (model 4505, Instron, High Wycombe, United Kingdom). The tensile modulus (E), σ_y, and the yield strain (ϵ_y) were determined at 23°C and 50% relative humidity according to procedures described in ISO 527-2. However, differing from this standard, rectangular specimens (170 mm × 12 mm × 4 mm, 12 mm corresponding to the thickness of the compression-molded plaques) were machined.

CCG tests under static loads

Crack growth experiments based on the principles of linear elastic fracture mechanics were performed under static loads at 60 and 80°C in distilled water in a test apparatus designed and constructed at the Institute of Materials Science and Testing of Plastics (University of Leoben, Leoben, Austria).[60,61] A schematic drawing of the test setup is shown in Figure 1(a). The tests were performed with specimens of the compact-type (CT) configuration,[62] which were machined from the compression-molded plaques. The geometry and size of the CT specimens are depicted in Figure 1(b). All specimens were kept at a controlled temperature of 23°C and 50% relative humidity for at least 14 days before the testing. To introduce precracks into the specimens before the fracture mechanics experiments, we slowly pressed a fresh commercial razor blade with a nominal thickness of 0.1 mm into the specimens at room temperature. The specimens were loaded with dead weights according to a specified initial K_I value, and the crack length at the specimen side surface and the crack opening displacement at the specimen front edge were measured with a travelling microscope at a magnification of 30×.

For the relevant test configuration, K_I was calculated according to the following expression:[62]

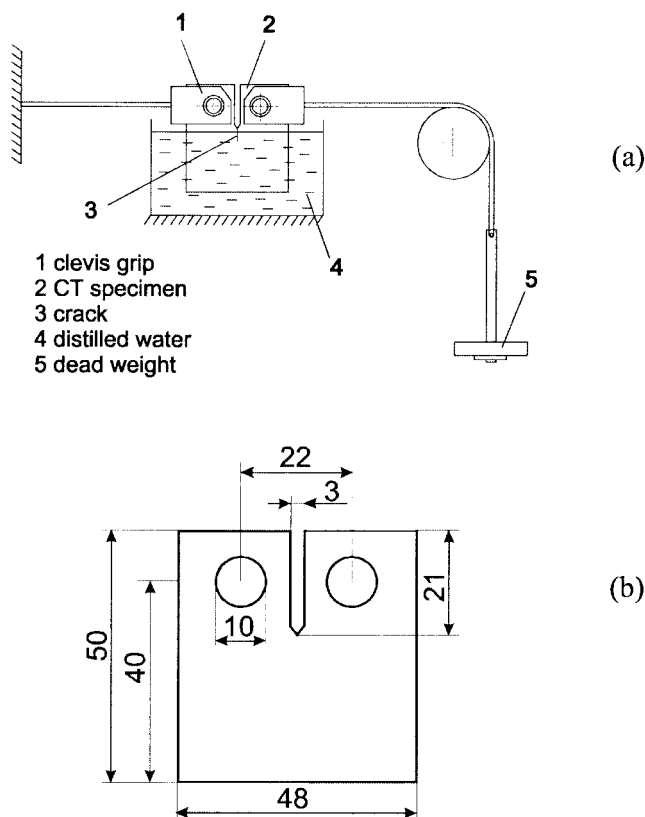$$K_I = \frac{F}{B\sqrt{W}} f\left(\frac{a}{W}\right) \qquad (2)$$

Figure 1 CCG testing under static loads: (a) test setup and (b) specimen type and geometry (dimensions in millimeters).

where F is the applied load, B is the specimen thickness, W is the specimen width, and a is the crack length; $f(a/W)$ is a nondimensional correction function that accounts for the specimen configuration and geometry and the loading conditions.

Values for CCG initiation times were determined from measurements of the crack opening displacement at the specimen front face (COD$_{ff}$) as a function of the loading time. By the plotting of COD$_{ff}$ data as a function of the loading time in a double logarithmic diagram, the point of crack initiation corresponds to the first deviation of these data from the linear base line. The CCG initiation times so determined were found to be in good agreement with travelling microscope observations of the immediate crack tip region. After the CCG initiation period, crack growth rates (da/dt) were calculated with a method analogous to that proposed in ASTM E 647-93 for the determination of fatigue crack growth. This method for computing da/dt involves fitting a second-order polynomial (parabola) to sets of successive data points of the crack length and time. The rate of crack growth is obtained from the slope of the parabola.

Further details of the test apparatus, the test procedure, and the data reduction are described elsewhere.[60,61]

TABLE III
Stabilizer Concentration in the Pellets and in the Compression-Molded Plaques Measured by HPLC

Polymer	Stabilization	antioxidant	Stabilizer concentration	
			Pellets (mass %)	Plaques (mass %)
PE-HD 1*	S	Santonox R	0.1	0.063
	K1	Irganox 1010	0.05	0.029
		Irgafos 168	0.05	0.017
		Irgafos 168 phosphate	—	0.033
	K2	Irganox 1010	0.1	0.061
		Irgafos 168	0.1	0.054
		Irgafos 168 phosphate	—	0.036
PE-HD 2*	S	Santonox R	0.1	0.07
	K1	Irganox 1010	0.05	0.035
		Irgafos 168	0.05	0.025
		Irgafos 168 phosphate	—	0.019
	K2	Irganox 1010	0.1	0.068
		Irgafos 168	0.1	0.062
		Irgafos 168 phosphate	—	0.030

Fractographic investigations

The investigations of specific fracture surface details were carried out with scanning electron microscopy (SEM; Zeiss, Oberkochen, Germany). All specimens were sputter-coated with a 15–20-nm-thick layer of gold. The operating voltage was 10 kV.

RESULTS AND DISCUSSION

Molecular and morphological material characterization

Stabilizer concentration

Although the various material formulations were compression-molded at a rather low maximum temperature of 180°C, some consumption of stabilizers during processing had to be expected. As illustrated by the results in Table III, a considerable drop in the stabilizer concentrations was detected when we compared the stabilizer mass contents of compression-molded plaques determined by HPLC analysis with the original concentrations of the compound process. However, in this context, it must be mentioned that with the HPLC method applied, only that part of the

multifunctional phenolic antioxidants is detected, of which none of the phenolic groups has reacted. In other words, if only one of the phenolic groups has reacted, a stabilizer molecule is no longer detected by the HPLC technique used, although the remaining phenolic groups are still active. Alternatively, in the case of the secondary antioxidant Irgafos 168 in the stabilization system K, both the original phosphite and its reaction product upon aging, that is, the corresponding phosphate of Irgafos 168, can be determined quantitatively.

For a given polyolefin/stabilizer compound, the OIT values and, although significantly less sensitive, the T_{ox} values are frequently used as a measure for changes in the active stabilizer concentration (i.e., including all residual functional groups in stabilizers) due to the exposure of compounds to different thermal and environmental histories.[63–66]

OIT values and T_{ox} values determined for the various material formulations on pellets and plaques are listed in Table IV. Although in terms of T_{ox} hardly any difference was observed between the material states in pellets and plaques, a comparison of OIT values for the two material states indicated some reduction in the

TABLE IV
Comparison of OIT and T_{ox} Values of Pellets and Compression-Molded Plaques

Polymer	Stabilization	OIT (180°C) (min)		T_{ox} (°C)	
		Pellets	Plaque	Pellets	Plaque
PE-HD 1*	S	720	630	259	258
	K1	750	500	244	244
	K2	2230	1620	255	252
PE-HD 2*	S	710	705	261	261
	K1	630	500	234	231
	K2	1890	1640	253	249

active stabilizer concentration for each of the compounds upon the processing of pellets into plaques by compression molding. However, the changes in the OIT values were of the same order for all formulations, and so it may be concluded that all the material compounds investigated were affected in a similar way by the compression-molding processing conditions at elevated temperatures. Specifically, the comparison of polymer/stabilizer formulations K1 and K2, for which the same stabilizer system was used, indicated that the relative difference in the stabilizer concentrations on the pellet level was in a first approximation fully transferred to the plaque level. As the changes in the OIT values from the pellet state to the plaque state are considered not untypical for such processing conditions, it may be assumed that the stabilization in the plaques of all the formulations was still nearly fully intact and that no oxidative degradation of the polymers occurred upon processing.

Rheological properties

The results of the rheological investigations, used to characterize any differences in the molecular masses and molecular mass distributions of the various formulations, are shown later for PE-HD 1* and PE-HD 2* in Figures 3 and 4, respectively. As pointed out previously, the samples and specimens for these tests were taken from compression-molded plaques to characterize the molecular states of the various materials before CCG testing.

For PE-HD1* formulations, curves of η^* at 150°C are depicted as a function of frequency in Figure 2(a). Because of the low average molecular mass and the rather narrow molecular mass distribution of the base polymer, η^*_0 was discernible for all formulations for frequencies lower than 1 rad/s. Although the viscosity curves of the formulations S, K1, and K2 were identical within the reproducibility range of this test, the unstabilized base polymer PE-HD 1*/0 exhibited slightly higher viscosities over the entire frequency range, indicating somewhat higher values in the mean molecular mass. The higher average molecular mass of the unstabilized base polymer was probably due to branching and crosslinking reactions during compression molding, phenomena that have been observed by others for unstabilized or poorly stabilized PEs as well.[45]

The frequency dependence of G' and G'' values is shown in Figure 2(b,c), the latter diagram being a magnification of the crossover region in Figure 2(b). The close positions of the G_c values of the formulations S, K1, and K2 indicate again that the base polymer in all three of these formulations was identical in terms of both the molecular mass and molecular mass distribution. However, the slight shift of G_c of the unstabilized polymer PE-HD1*/0 toward lower frequencies implies an increase in the mean molecular mass, which is in good agreement with the interpretation of the observed increase in η^* previously described.

All of these results, along with the corresponding interpretations, were corroborated by the shear stress relaxation modulus dependence on time of these materials, which is depicted in Figure 2(d). Although identical curves were again obtained for the formulations S, K1, and K2, the unstabilized polymer exhibited a slightly lower stress relaxation tendency.

In a similar fashion, the results for the stabilizer formulations with the base polymer PE-HD 2* are presented in Figure 3. Again, no differences were discernible between the various stabilizer formulations of this polymer type with S, K1, and K2, in terms of both linear (shear viscosity and shear modulus frequency dependence) and nonlinear viscoelastic (shear stress relaxation modulus) rheological properties.

Morphology and microstructure

An overview of the experimental results related to the morphologies and microstructures of the various compounds is provided in Table V. With the DSC method, some difference in the overall X_c was detected for the PE-HD formulations of the two base polymers (81% for formulations of PE-HD 1* and 76% for formulations of PE-HD 2*). However, for a given base polymer type, these overall values of X_c were found to be independent of the stabilizer type and content. These DSC results were confirmed by the results of density measurements. The higher values of density in Table V, compared with the data from the data sheets of the manufacturer (Borealis AG; cf. Table I), resulted from the slow-cooling process after the compression molding of the plaques.

Similarly, for a given base polymer type, the crystalline fine structure investigated by SAXS measurements also was found to be largely independent of the stabilizer type and content, at least in terms of the distribution of L_c. Comparing the two base polymer types, we obtained average L_c values of 24.0 and 21.8 nm for PE-HD 1* and PE-HD 2* formulations, respectively, with all L_c distributions exhibiting a distinguished uniformity [see Fig. 4(a,c)]. With respect to the thickness of the disordered (amorphous) top layers, no effect of stabilization was found for the PE-HD 2* formulations [see Fig. 4(d)], whereas some influence was noticed for PE-HD 1* formulations, with the formulations K1 and K2 exhibiting somewhat broader thickness distributions than formulation S [see Fig. 4(b)].
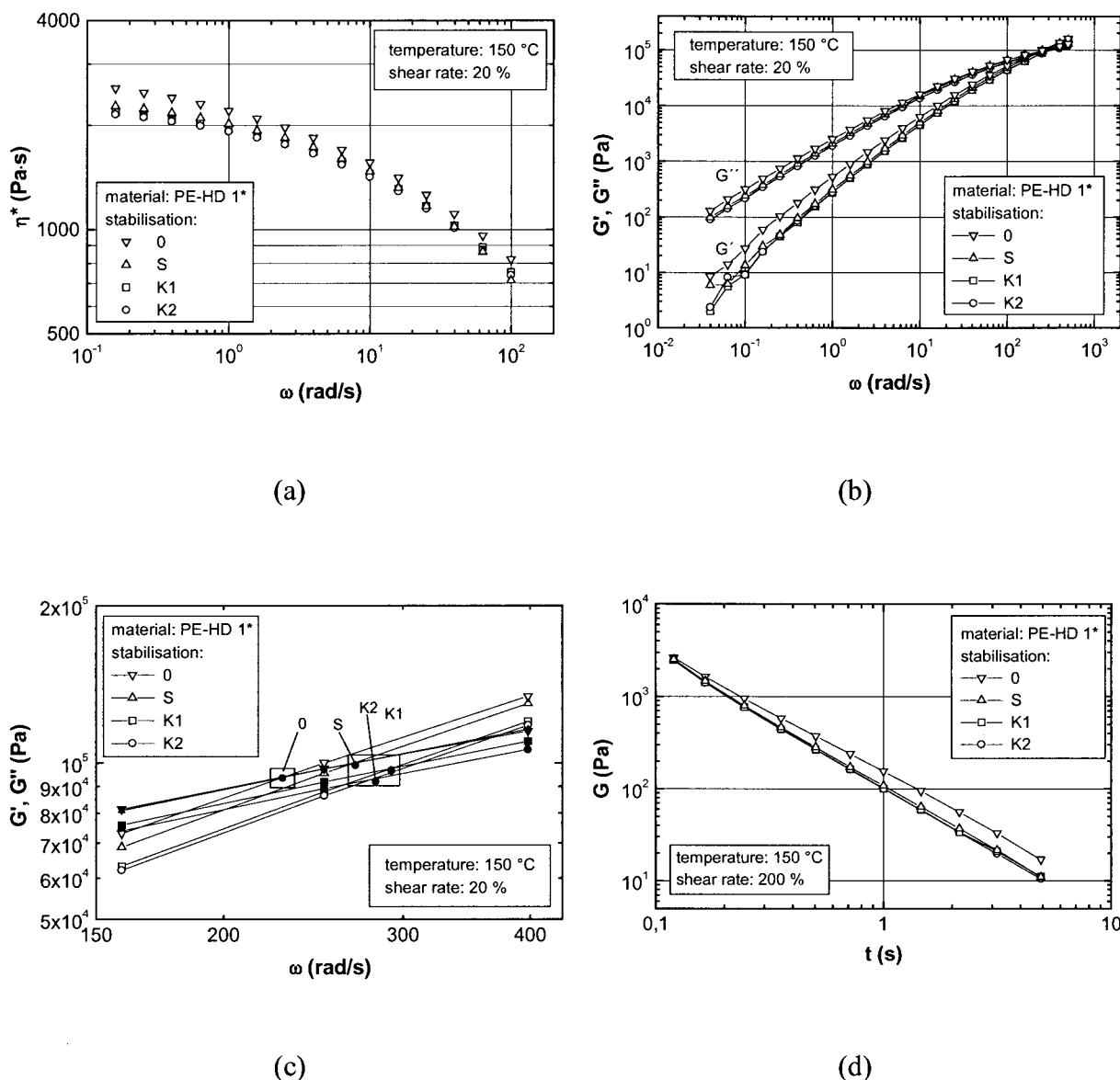
(a)

(b)

(c)

(d)

Figure 2 Rheological properties of the formulations of PE-HD 1*: (a) η^* as a function of ω, (b) G' and G'' as functions of ω, (c) G_c , and (d) the stress relaxation modulus (G) as a function of time t.

Interim conclusions regarding molecular and morphological material characterization

Overall, the following conclusions may be drawn with respect to the molecular and morphological characteristics of the various material formulations included in this study:

- Compared to PE-HD 1*, PE-HD 2* exhibits higher values for the mean molecular mass (weight average) and a broader molecular mass distribution. However, for a given base polymer, the mean molecular masses and molecular mass distributions of stabilized compounds are largely independent of the stabilizer type and content.
- For the unstabilized polymer PE-HD 1* (i.e., formulation PE-HD 1*/0), somewhat higher values for the

mean molecular mass were found in compression-molded plaques, indicating a certain degree of branching and crosslinking during processing.

- A certain amount of stabilizer consumption during the compression molding of plaques was detected for all stabilized formulations, the relative magnitude being about equal for all compounds. Thus, the ranking in terms of the degree of stabilization in the compounding process and in pellets and plaques remained about equal.
- Compared with PE-HD 1*, PE-HD 2* exhibited a lower value of X_c, with lower values for L_c and the average thickness of amorphous top layers (L_a). However, for a given base polymer, the morphological fine structure was largely independent of the stabilizer type and content.
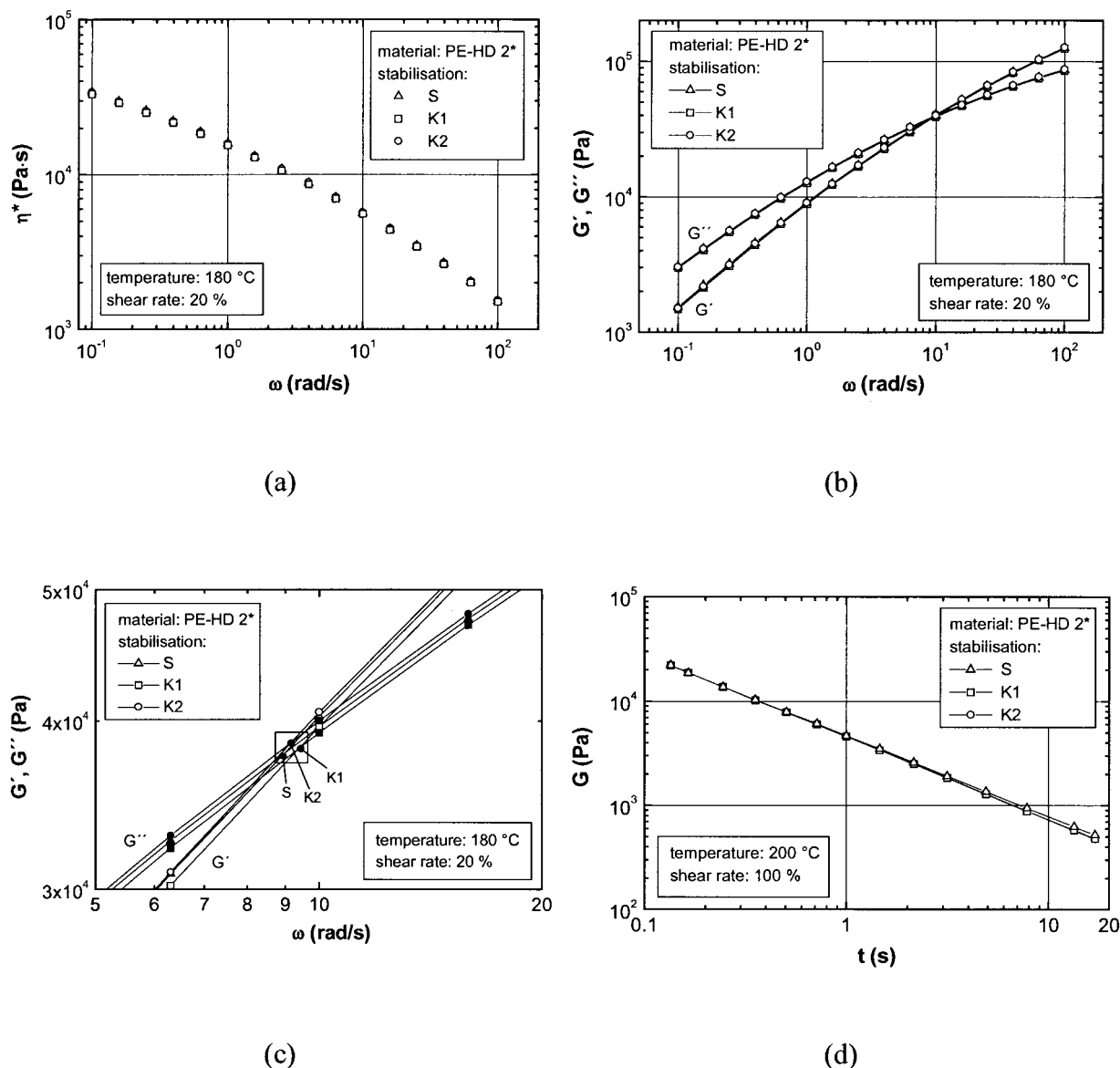
(a)

(b)

(c)

(d)

Figure 3 Rheological properties of the formulations of PE-HD 2*: (a) η^* as a function of ω, (b) G' and G'' as functions of ω, (c) G_c, and (d) the stress relaxation modulus (G) as a function of time t.

Mechanical material properties

Some basic mechanical properties of all the compounds investigated are listed in Table VI, which also indicates the densities of the various formulations. As expected from the material density, somewhat higher values for E and σ_y and lower values for the ϵ_y were found for formulations of PE-HD 1*. However, in good agreement with the results of the molecular, morphological, and microstructural investigations, all tensile properties of the formulations with a given base polymer were found to be independent of the stabilizer type and content. Also corroborating the rheological results, from which it was concluded that some branching and crosslinking may have occurred during compression mold-

TABLE V
Morphological and Microstructural Characteristics of the Various Compounds in the State of Compression-Molded Plaques

Polymer	Stabilization	X_c (%)	ρ (g/cm³)	L_c (nm)	L_a (nm)
PE-HD 1*	0	80.5	0.969	—	—
	S	81.0	0.971	23.7	5.0
	K1	81.5	0.971	24.2	4.7
	K2	81.0	0.971	24.1	4.9
PE-HD 2*	S	77	0.963	21.9	3.6
	K1	76	0.963	21.5	3.7
	K2	75	0.962	22.1	3.7

ρ = density, Defined according to ISO 1183 at 23°C and 50% relative humidity.
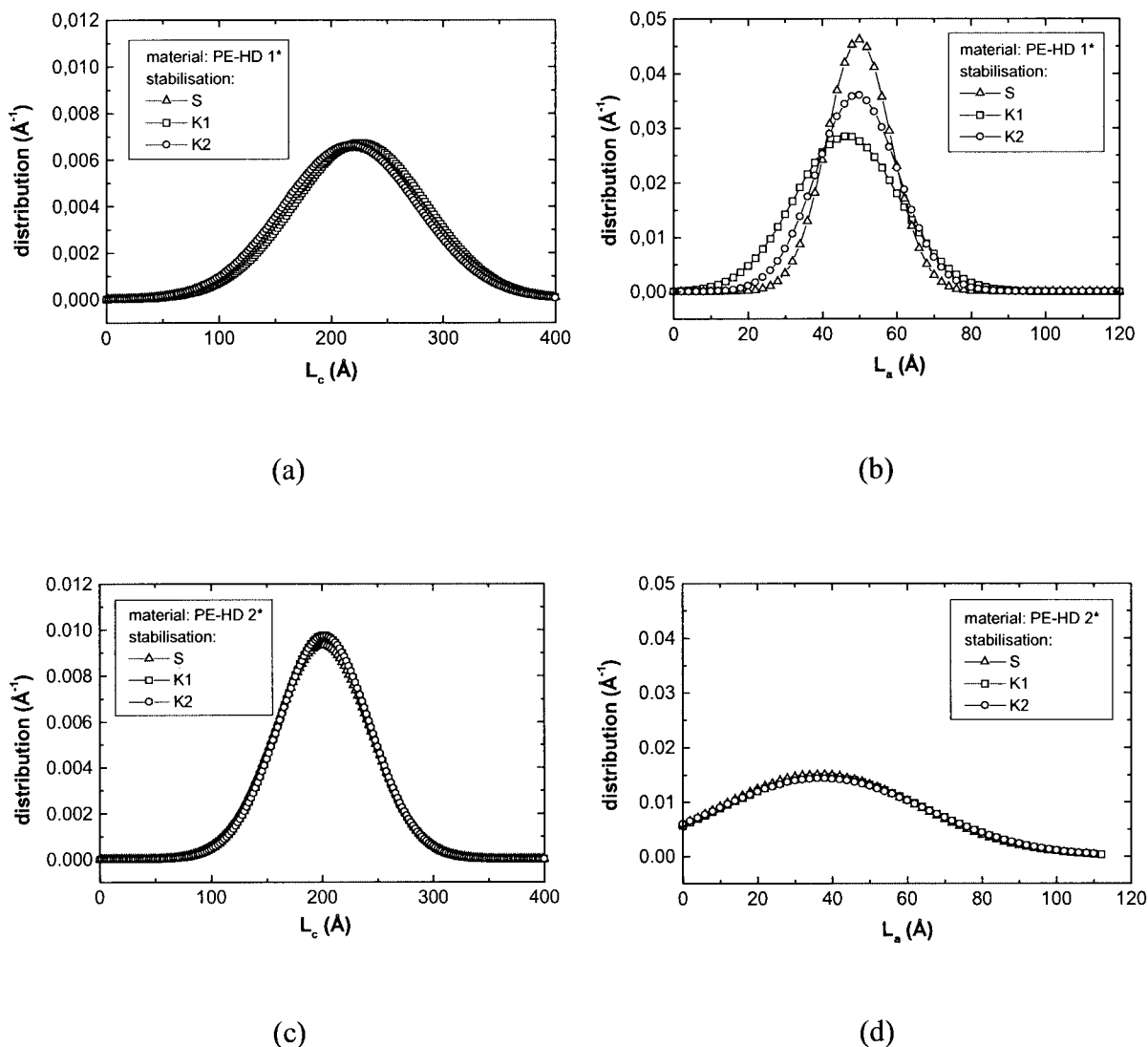
(a)

(b)

(c)

(d)

Figure 4   (a,c) Distributions of L_c and (b,d) distributions of L_a for the different formulations of PE-HD 1* and PE-HD 2*, respectively.

ing of the unstabilized material PE-HD 1*/0, were the slightly higher and lower values for E and ϵ_y, respectively, of this material.

TABLE VI
Comparison of Density (ρ) and Mechanical Properties of the Compression-Molded Plaques Measured at 23°C and 50% Relative Humidity

Polymer	Stabilization	ρ (g/cm^3)	E (MPa)	σ_y (MPa)	ϵ_y (%)
PE-HD 1*	0	0.969	1782	32	8.3
	S	0.971	1735	32	9.1
	K1	0.971	1755	32.2	9.3
	K2	0.971	1770	32.4	9.4
PE-HD 2*	S	0.963	1400	30.1	10.2
	K1	0.963	1420	29.3	10.4
	K2	0.962	1365	29.7	10.3

ρ was defined according to ISO 1183

CCG behavior under static loads

An extensive CCG initiation time that depends on the precracking procedure, the value of the initial K_I level, and the test temperature[5,6,67,68] may precede stable CCG in PE-HD. CCG initiation is characterized by the breakdown of the fibrillar microstructure at the base of the plastic deformation zone (craze) that develops at the crack tip upon specimen loading.[3,69]

For a given set of test conditions and in comparison with compounds of PE-HD 1*, formulations of PE-HD 2* in general exhibited longer CCG initiation times. Interestingly, however, no clear differences in the CCG initiation times could be detected for the various formulations of a given base polymer. This may at least be due in part to difficulties in precisely determining the point of CCG initiation, and further research is needed to examine the role of stabilizers in the CCG initiation stage.
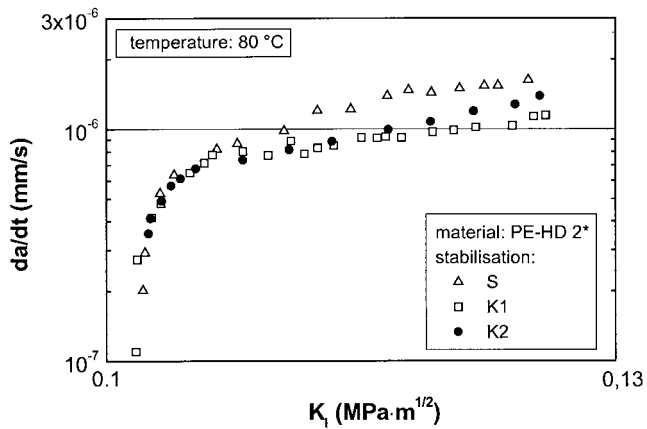
Figure 5 Transient CCG followed by quasiequilibrium CCG for the formulations of PE-HD 2*.

Once CCG commences and after an initial period of crack acceleration (transient crack growth[5]), the so-called equilibrium crack growth stage is reached,[70] in which the influence of stabilization becomes more pronounced. This transition from the CCG initiation stage to the CCG propagation stage is shown for the various formulations of PE-HD 2* for a test temperature of 80°C in Figure 5.

The equilibrium curves of CCG rates for test temperatures of 60 and 80°C and the effects of stabilization for a given base polymer type are shown in Figures 6 and 7, respectively, for PE-HD 1* and PE-HD 2*. On the basis of these illustrations, the following general observations may be made:

- The most significant influence of stabilization was observed at low CCG rates, with CCG curves of the various formulations of a given polymer type converging at high CCG rates.
- In the regime of low CCG rates, formulations with the stabilizer S exhibited the highest CCG rates, and formulations with the stabilizer K1 exhibited the lowest CCG rates. It should be mentioned that even minor effects of different stabilizer systems or stabilizer concentrations on CCG rates, particularly at low crack growth rates, translate into significant improvements in lifetimes of pressurized pipes (these results corroborate investigations on pressurized pipes in terms of material ranking[28]).

Because the total time period of the CCG experiments lay within a few weeks, the global aging of the entire fracture mechanics test specimens may be excluded as cause for these observations. Indeed, T_{ox} and OIT values, which were determined from samples of CT specimens after the completion of the CCG tests at 60 and 80°C, showed no measurable alterations with respect to the values of corresponding samples

obtained from unexposed plaques. Hence, on a global specimen scale, the loss of stabilizers by reactive consumption or by diffusion and extraction into the surrounding water during a CCG experiment may be regarded as negligible.

As global aging may thus be disregarded in explaining the phenomena observed, the influence of stabilizers for a given base polymer at low CCG rates is believed to be a result of local aging around the crack tip related to the combined influence of time, the elevated temperature, the presence of oxygen and water, and the high mechanical stresses in the immediate crack tip region (see Fig. 8). In this context, it is important to recognize that the damage zone ahead of the crack front consists of highly drawn, crazelike deformation zones of porous material structure with a high surface-to-volume ratio and thus is open to chemical and oxidative attacks as well as increased
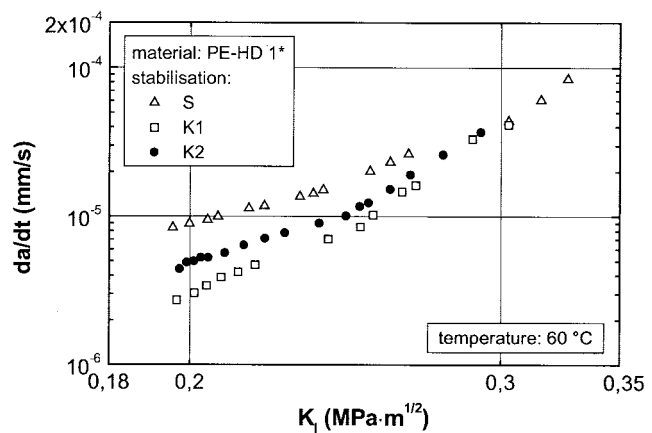
(a)
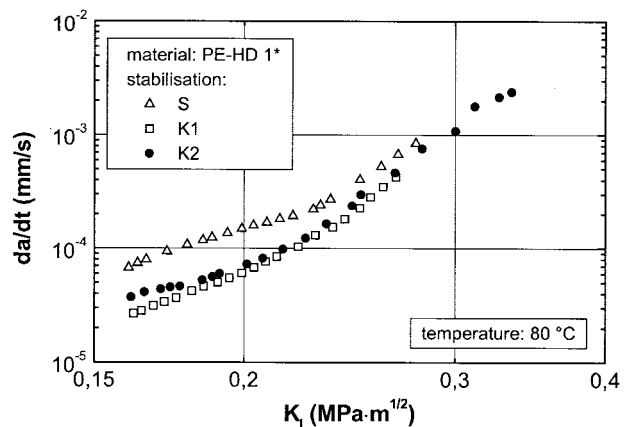
(b)

Figure 6 CCG behavior of the formulations of PE-HD 1* under equilibrium conditions at (a) 60 and (b) 80°C.
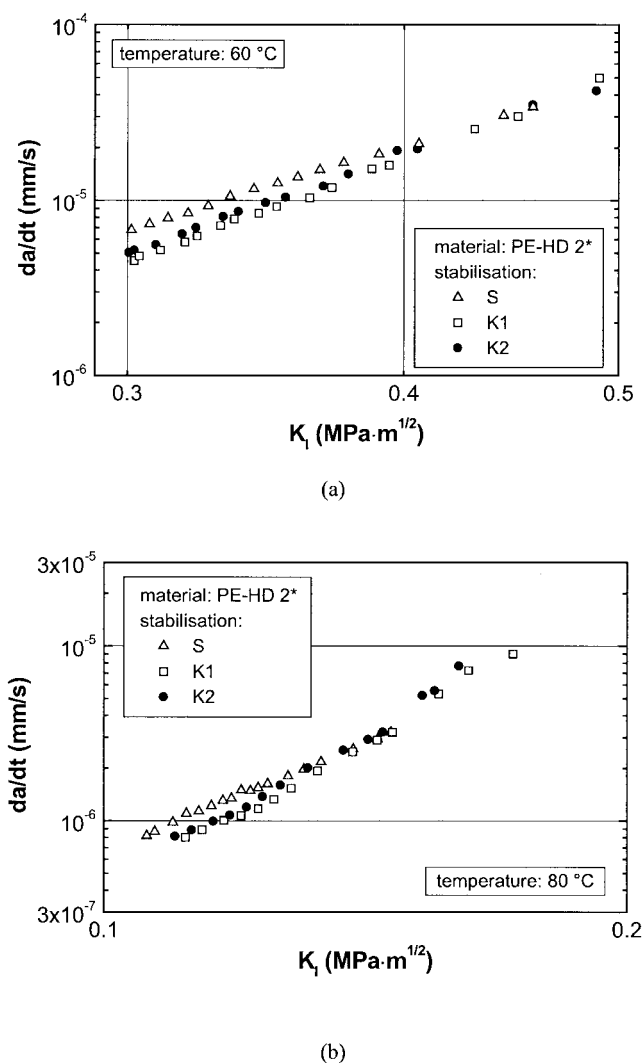
Figure 7 CCG behavior of the formulations of PE-HD 2* under equilibrium conditions at (a) 60 and (b) 80°C.

extractability of stabilizers. As CCG rates are very sensitive to molecular and morphological changes, this local aging process may well influence CCG rates, particularly when the density of tie molecules and interlamellar entanglements in the crack tip region is affected.

In this context, other authors[50] have shown analogous effects in demonstrating that notched PP samples under creeplike loading conditions fail in a shorter time when simultaneously exposed to ultraviolet radiation. As stabilizers delay the autoxidation and degradation of the polymer, they should also be effective near the tip of the growing crack and thus should influence local aging and CCG rates. The fact that all the curves converge at higher crack growth rates corroborates the influence of local aging on CCG. As the timescale for local aging is reduced at high crack speeds, the CCG curves of the different formulations in Figures 6 and 7 converge at high K_I values.

To provide further evidence for the enhanced tendency of local oxidative degradation in the immediate crack tip region, we determined the concentrations of carbonyl groups on the fracture surfaces of CCG specimens via infrared spectroscopy and compared our findings with the results of such investigations obtained from other specimen surfaces as references. Infrared spectra of crack surfaces and specimen side surfaces of CT specimens of the formulations of both PE-HD base polymers tested at 60°C are shown within a range of wave numbers from 1600 to 2100 cm^{-1} in Figures 9 and 10. The carbonyl groups exhibited their typical absorption bands within wave numbers of 1700–1740 cm^{-1}. The absorption band at 2020 cm^{-1} was always present in PE, and so the ratio of this peak to the absorption peak of the carbonyl groups could be used as a measure for the degree of oxidation. The comparison of the crack surface and reference surface infrared spectra for each of the materials indicated that the oxidation was enhanced by the local stress concentration in the area of the cracks. Thus, although these results did not allow for any quantitative estimates of the degree of local oxidation, particularly for the comparison of different formulations, they corroborated the argument of enhanced local aging in the immediate crack tip region. Further investigations with an infrared microscope and with attenuated total reflectance spectroscopy are in progress and should provide more detailed information in the near future.

Surprisingly, stabilizer K1, containing the same antioxidants as K2 but in lower concentrations, showed the highest crack growth resistance (see Figs. 6 and 7). Although further studies are needed to clarify the mechanisms involved, the following explanations seem possible. Brittle failure can be initiated by morphological defects. Low-molecular-weight additives, chain ends, branches, foreign material, and other noncrystallizable components are distributed primarily within the amorphous zones between the lamellae and are responsible for locally weakened areas with a re-
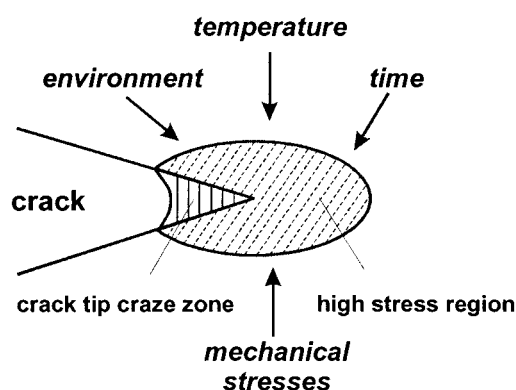

Figure 8 Schematic illustration of the crack tip region in PE-HD and the parameters controlling local crack tip aging.
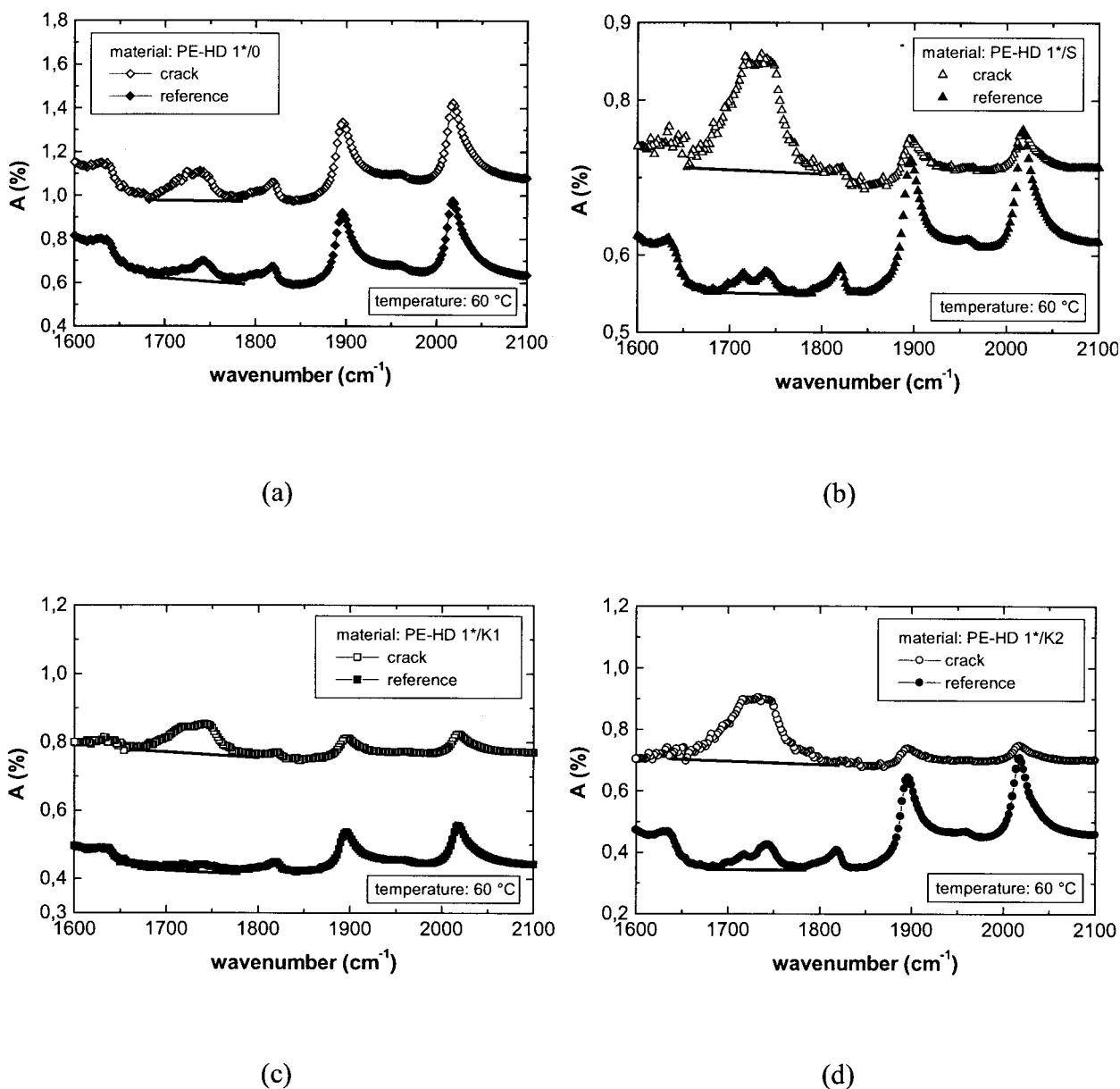
Figure 9 Comparison of the infrared absorption spectra of the fracture surfaces and side surfaces of CT samples of PE-HD 1* tested at 60°C: (a) PE-HD 1*/0, (b) PE-HD 1*/S, (c) PE-HD 1*/K1, and (d) PE-HD 1*/K2.

duced tie molecule concentration[71,72] and thus preferentially become places for crack growth initiation and crack growth. Stabilizers also belong to this group of additives, which are soluble only in the amorphous regions and may possibly favor crack growth to a certain extent.

Alternatively, changes in the molecular and morphological structure (i.e., branching, crosslinking, and lamellar thickness) during processing may also serve as possible explanations for the anomalistic behavior of compounds with K1 or K2. Although no differences in the molecular mass distribution and crystalline morphology could be detected, any changes on an extreme local or molecular scale beyond the sensitivity

of the characterization methods used (i.e., HPLC, rheological analyses, thermoanalytical analyses, and SAXS) cannot totally be excluded. In other words, it may be that the lower concentration of the stabilizer in K1 compounds resulted in a somewhat higher degree of effective tie molecule and interlamellar entanglement density after the exposure to the various processing conditions (compression molding of CT specimens), and this led to enhanced crack growth resistance.[6-9]

Another interesting aspect of this investigation is shown in Figure 11, which compares the CCG curves of various PE-HD 1* stabilizer formulations with the CCG curve of the unstabilized base polymer. Accord-
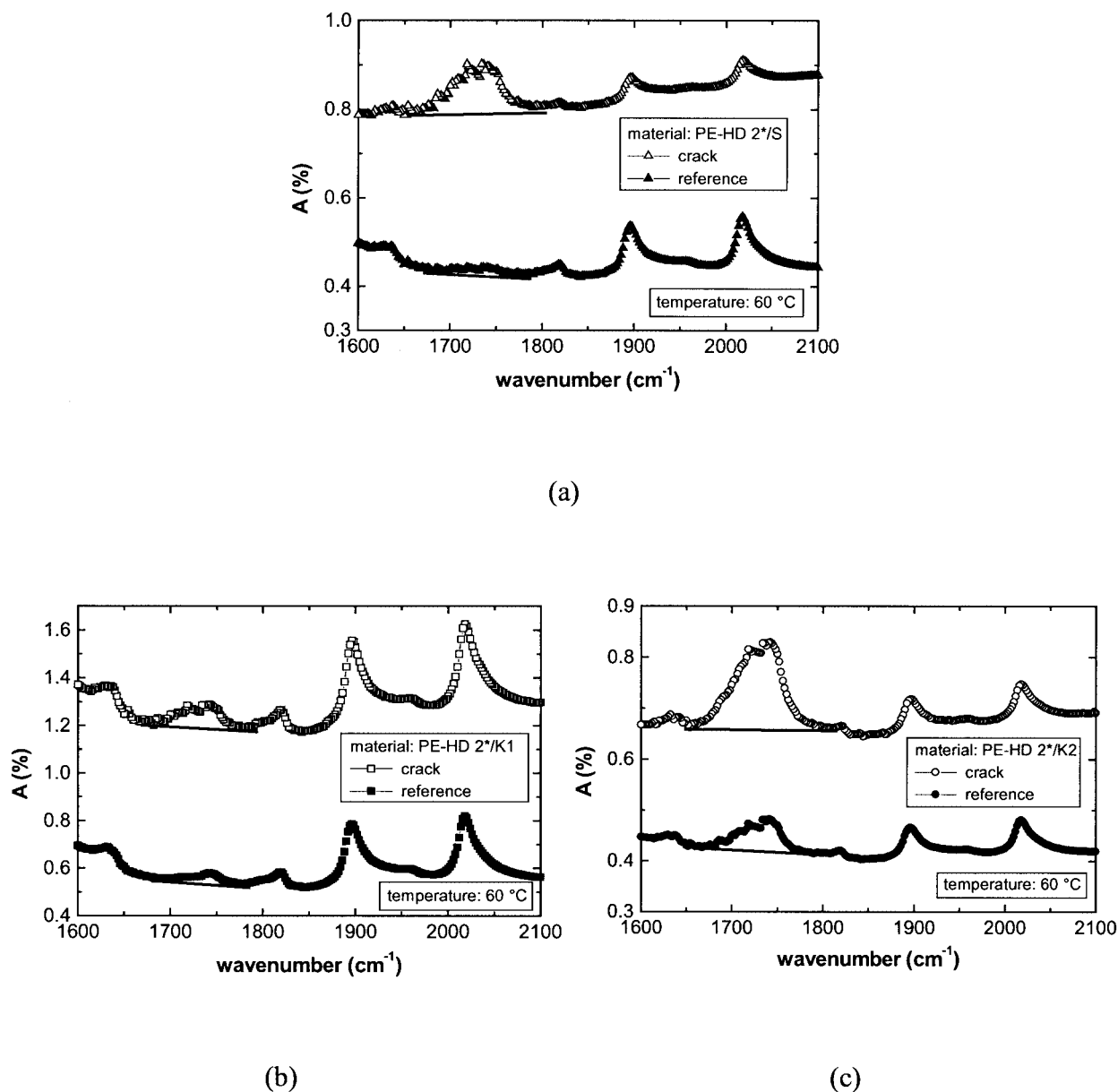
(a)

(b)

(c)

Figure 10 Comparison of the infrared absorption spectra of the fracture surfaces and side surfaces of CT samples of PE-HD 2* tested at 60°C: (a) PE-HD 2*/S, (b) PE-HD 2*/K1, and (c) PE-HD 2*/K2.

ing to these diagrams, the crack growth rates of the unstabilized formulation PE-HD 1*/0 in the low CCG rate regime, although higher than those of the K1 and K2 formulations, were reduced with respect to that of the stabilized compound PE-HD 1*/S. This relative improvement of unstabilized PE-HD 1*/0 in comparison with the stabilized formulation PE-HD 1*/S is believed to be due to the occurrence of branching and crosslinking in the unstabilized material during compression molding, as previously described on the basis of rheological investigations. This again emphasizes the important role of molecular parameters, which are treated in more detail elsewhere.[6–9]

Fracture surface analysis

In the following, comparisons of CCG fracture surfaces are made with SEM images for equivalent K_I values, as K_I is known to control the size of the plastic zone (r_y) both in length and thickness directions $(r_y \propto K_I^2/\sigma_y^2)$. K_I, therefore, should also control the irreversible material deformations at the crack tip. In Figure 12, the fracture surfaces of PE-HD 1*/K2 and PE-HD 2*/K2 are compared at 60°C and a K_I value of 0.33 MPa $m^{1/2}$. Although the fracture surface of PE-HD 2*/K2 in Figure 12(b) is characterized by remnants of highly stretched fibrils, reflecting the higher ductility
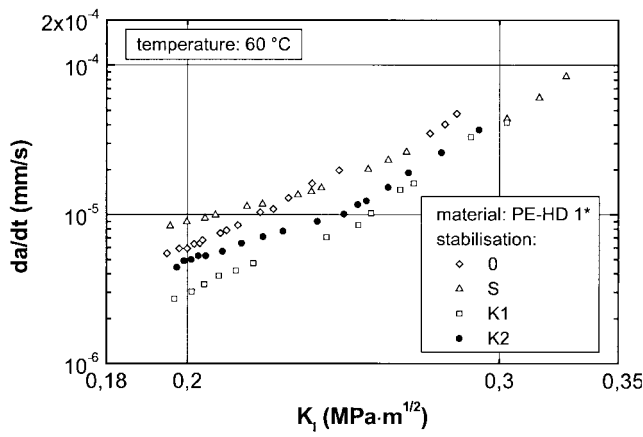
(a)
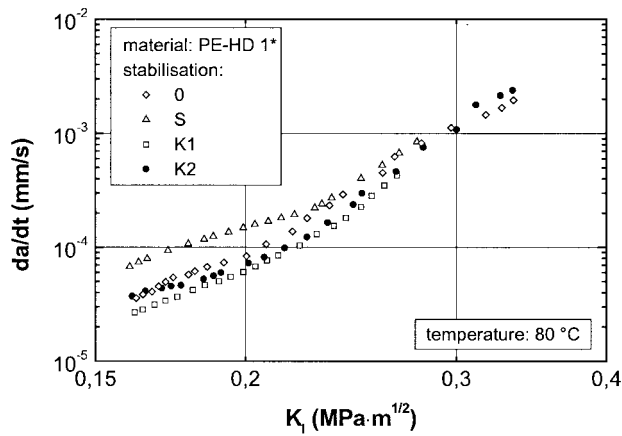
(b)

Figure 11 Influence of crosslinking during processing on the CCG behavior of PE-HD 1/0 under equilibrium conditions at (a) 60 and (b) 80°C.

associated with the enhanced tie molecule density of this higher molecular mass material, much less ductile deformation is seen in Figure 12(a) for the lower molecular mass material PE-HD 1*/K2.
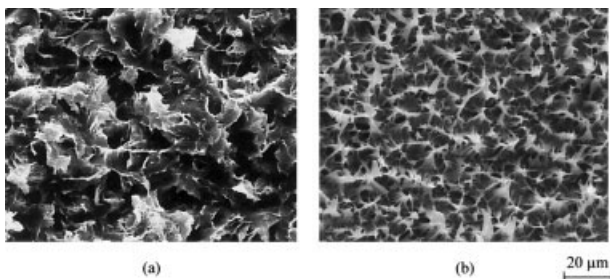

Figure 12 Comparison of the fracture surfaces of the two PE-HD types investigated and tested at 60°C and $K_I = 0.33$ MPa m$^{1/2}$: (a) PE-HD 1*/K2, $da/dt = 8.5 \times 10^{-5}$ mm/s, and (b) PE-HD 2*/K2, $da/dt = 7 \times 10^{-6}$ mm/s.
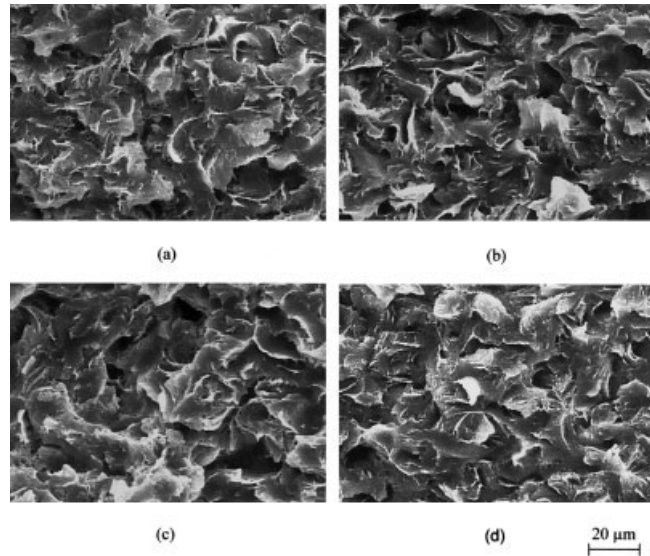

Figure 13 Comparison of the fracture surfaces of the different formulations of PE-HD 1* tested at 60°C and $K_I = 0.2$ MPa m$^{1/2}$: (a) PE-HD 1*/0, $da/dt = 6 \times 10^{-6}$ mm/s; (b) PE-HD 1*/S, $da/dt = 9 \times 10^{-6}$ mm/s; (c) PE-HD 1*/K1, $da/dt = 3 \times 10^{-6}$ mm/s; and (d) PE-HD 1*/K2, $da/dt = 5 \times 10^{-6}$ mm/s.

Fracture surface images of PE-HD 1* and PE-HD 2* containing different stabilizers and tested at 60°C are shown in Figures 13 and 14, respectively. For a given base polymer, virtually no influence of stabilization can be discerned. The lack of any stabilizer effect on the fracture surface appearance for a given level of K_I, for which crack growth rates were found to vary at
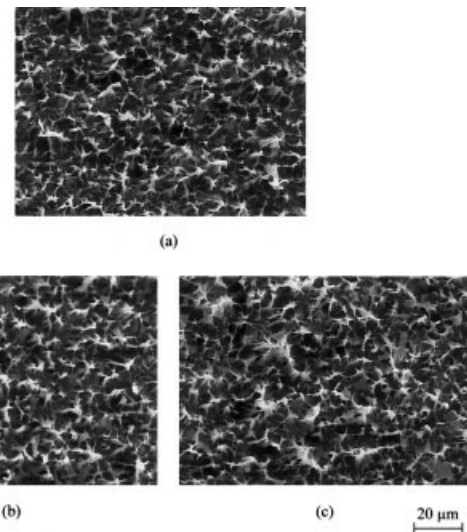

Figure 14 Comparison of the fracture surfaces of the different formulations of PE-HD 2* tested at 60°C and $K_I = 0.3$ MPa m$^{1/2}$: (a) PE-HD 2*/S, $da/dt = 7 \times 10^{-6}$ mm/s; (b) PE-HD 2*/K1, $da/dt = 4.2 \times 10^{-6}$ mm/s; and (c) PE-HD 2*/K2, $da/dt = 5 \times 10^{-6}$ mm/s.

least to some degree according to the stabilizer/stabilizer system, may be explained as follows. Both plastic zone formation and plastic zone breakdown at the crack tip depend on a complex interaction of molecular (average molecular mass and molecular mass distribution of the polymer and stabilizer type and content) and morphological (X_c and lamellar dimensions) parameters. According to concepts of fracture mechanics,[73] plastic zone formation, including the tendency for highly stretched fibril formation, is believed to depend on all parameters that affect yield and postyield behavior (X_c and tie molecule density via lamella dimensions and molecular mass distribution). As the stabilizer system was shown to have no effect on any of these parameters for a given base polymer (see the previous sections), the features of remnants of plastic deformation zones on fracture surfaces are also largely unaffected by the stabilizer system. Plastic zone breakdown, however, at least in the low crack growth regime, is believed to additionally depend on local crack tip aging processes and is thus affected by the type and degree of stabilization leading to stabilizer-dependent CCG rates. These local crack tip aging processes take place in the already stretched crack tip craze fibril network on a molecular scale and are, therefore, not visible on SEM fracture surfaces.

CONCLUSIONS

A linear elastic fracture mechanics test methodology was applied to characterize the influence of stabilization (three different stabilizer systems designated S, K1 and K2) on the kinetics of CCG initiation and CCG rates of two PE-HD types in distilled water under static loads at 60 and 80°C. In both PE-HD types, crack growth rates were found to depend on the stabilizer system, particularly in the low CCG regime, with diminishing stabilizer effects at higher CCG rates.

For a given PE-HD type, no molecular and morphological differences between the formulations containing various stabilizers could be detected. Hence, the phenomena observed were explained in terms of local aging processes in the immediate vicinity of the crack tip, which were controlled by the presence and contents of various stabilizers. The concept of local crack tip aging assumes that the high stresses approaching the material yield and craze stress in the immediate vicinity of the crack tip assist and accelerate the thermooxidative degradation of the material.

As stabilizers in general act to delay the autoxidation and degradation of a polymer, they should also be effective near the tip of the growing crack and thus influence local aging processes and hence the crack tip plastic zone breakdown process and CCG rates. Depending on the crack growth rate (and, therefore, the applied value of K_I) and on the stabilizer type, this effect will be more or less pronounced. At high crack speeds, at which there was not enough time for local degradation reactions, the curves of the variously stabilized PE-HD materials converged. The hypothesis of local crack tip aging was supported by measurements of the carbonyl concentration. That is, in comparison with the remaining sections of the CCG specimens investigated, a significantly higher concentration of carbonyl groups was detected on CCG fracture surfaces.

References

1. Chan, M. K. V.; Williams, J. G. Polymer 1983, 24, 234.
2. Fleißner, M. Kunststoffe 1987, 77, 45.
3. Brown, N.; Lu, X.; Huang, Y.; Qian, R. Makromol Chem Macromol Symp 1991, 41, 55.
4. Brown, N.; Lu, X. Polymer 1995, 36, 543.
5. Stern, A. Ph.D. Thesis, University of Leoben, 1995.
6. Pinter, G. Ph.D. Thesis, University of Leoben, 1999.
7. Brown, N.; Lu, X.; Huang, Y.; Harrison, I. P.; Ishikawa, N. Plast Rubber Compos Process Appl 1992, 17, 255.
8. Egan, B. J.; Delatycki, O. J Mater Sci 1995, 30, 3351.
9. Yeh, J. T.; Chen, G. Y.; Hong, H. S. J Mater Sci 1994, 29, 4104.
10. Gebler, H. Kunststoffe 1989, 79, 823.
11. Dörner, G.; Lang, R. W. 3R Int 1997, 11, 672.
12. Lang, R. W.; Pinter, G.; Stern, A. Proc Plast Pipes 2001, 11, 329.
13. Pinter, G.; Lang, R. W. Plast Rubber Compos 2001, 30, 94.
14. Popov, A.; Rapoport, N.; Zaikov, G. Oxidation of Stressed Polymers; Gordon & Breach: New York, 1991.
15. Scott, G. Polym Eng Sci 1984, 24, 1007.
16. Terselius, B.; Gedde, U. W.; Jansson, J. F. In Failure of Plastics; Brostow, W.; Corneliussen, R. D., Eds.; Hanser: Munich, 1973; p 273.
17. Costa, L.; Luda, M. P.; Trossarelli, L. Polym Degrad Stab 1997, 55, 329.
18. Popov, A.; Krysyuk, B. E.; Zaikov, G. Polym Sci USSR 1980, 22, 1501.
19. Popov, A.; Krysyuk, B. E.; Blinov, N. N.; Zaikov, G. Eur Polym J 1981, 17, 169.
20. Skrypnyk, I. D.; Hockstra, H. D.; Spoormaker, J. L. Polym Degrad Stab 1998, 60, 21.
21. Rapoport, N. Proc Int Conf Adv Stab Degrad Polym 1995, 17, 245.
22. Zhurkov, S. N.; Zakrevskyi, V. A.; Korsukov, V. E.; Kuksenko, A. F. J Polym Sci Part A-2: Polym Phys 1972, 10, 1509.
23. Bueche, F. J Appl Phys 1955, 26, 1133.
24. Lang, R. W.; Stern, A.; Dörner, G. Angew Makromol Chem 1997, 247, 131.
25. Audouin, L.; Langlois, V.; Verdu, J.; de Bruijn, J. C. M. J Mater Sci 1994, 29, 569.
26. White, J. R.; Turnbull, A. J Mater Sci 1994, 29, 584.
27. Horrocks, A. R.; Valinejad, K.; Crighton, J. S. Polym Degrad Stab 1994, 43, 81.
28. Dörner, G. Ph.D. Thesis, University of Leoben, 1994.
29. Gedde, U. W.; Ifwarson, M. Polym Eng Sci 1990, 30, 202.
30. de Bruijn, J. C. M. Ph.D. Thesis, Delft University, 1992.
31. Wunderlich, B. Macromolecular Physics; Academic: New York, 1976; Vol. 2.
32. Reich, L.; Stivala, S. S. Elements of Polymer Degradation; McGraw-Hill: New York, 1971.
33. Popov, A. A.; Blinov, N. N.; Krysyuk, B. E.; Zaikov, G. E. Polym Degrad Stab 1984, 7, 33.
34. DeVries, K. L., Hornberger, L. E. Polym Degrad Stab 1989, 24, 213.
35. Baumhardt-Neto, R.; de Paoli, M. A. Polym Degrad Stab 1993, 40, 53.

36. Baumhardt-Neto, R.; de Paoli, M. A. Polym Degrad Stab 1993, 40, 59.
37. Gedde, U. W.; Viebke, J.; Leijström, H.; Ifwarson, M. Polym Eng Sci 1994, 34, 1773.
38. Kramer, E. Ph.D. Thesis, University of Leoben, 1987.
39. Smith, G. D.; Karlsson, K.; Gedde, U. W. Polym Eng Sci 1992, 32, 659.
40. Richters, P. Macromolecules 1970, 3, 262.
41. Knight, L. B.; Calvert, P. D.; Billingham, N. C. Polymer 1985, 26, 1713.
42. Billingham, N. C. Macromol Chem Macromol Symp 1989, 28, 145.
43. Celina, M.; George, G. A.; Billingham, N. C. Polym Prepr 1993, 34, 262.
44. Gächter, R.; Müller, H. Kunststoffadditive; Hanser: Munich, 1990.
45. Zweifel, H. Stabilisation of Polymeric Materials; Springer-Verlag: Berlin, 1998.
46. Lang, R. W.; Pinter, G.; Stern, A. Proc Plast Pipes 2001, 11, 853.
47. O'Donnell, B.; White, J. R. J Mater Sci 1994, 29, 3955.
48. O'Donnell, B.; White, J. R. Polym Degrad Stab 1994, 44, 211.
49. Kelly, C. T.; Tong, L.; White, J. R. J Mater Sci 1997, 32, 851.
50. Kelly, C. T.; White, J. R. Polym Degrad Stab 1997, 56, 367.
51. Technical Information; Borealis AG: Linz, Austria, 1995.
52. Technical Information; Borealis AG: Linz, Austria, 1995.
53. Lohmeyer, S. Die Speziellen Eigenschaften der Kunststoffe; Expert Verlag: Grafenau, Germany, 1984.
54. Kulicke, W. M. Fließverhalten von Stoffen und Stoffgemischen; Hüthig & Hepf: Heidelberg, Germany, 1986.
55. Franck, A. J. P. Introduction to the Rheology of Thermoplastic Melts; Rheometrics: Piscataway, NJ, 1989.
56. Dealy, J. M.; Wissburn, K. F. Melt Rheology and Its Role in Plastics Processing; Van Nostrand Reinhold: New York, 1990.
57. Osaki, K. Rheol Acta 1993, 32, 429.
58. Zipper, P. Test Report; Abteilung für Physikalische Chemie der Polymere, Institut für Physikalische Chemie, Universität Graz: Graz, Austria, 1997.
59. Gugumus, F. Polym Degrad Stab 1996, 52, 131.
60. Stern, A.; Novotny, M.; Lang, R. W. Polym Test 1998, 17, 403.
61. Stern, A.; Asanger, F.; Lang, R. W. Polym Test 1998, 17, 423.
62. Murakami, Y. Stress Intensity Factors Handbook; Pergamon: Oxford, 1987; Vol. 1.
63. Marshall, D. I.; George, E. J.; Turnipseed, J. M.; Glenn, J. L. Polym Eng Sci 1973, 13, 415.
64. Foster, G. N. In Oxidation Inhibition in Organic Materials; Pospisil, J.; Klemschuk, P. K., Eds.; CRC: Boca Raton, FL, 1990; Vol. 2.
65. Bharel, R.; Anand, R. C.; Choudhary, V.; Varma, I. K. Polym Degrad Stab 1992, 38, 107.
66. Karlsson, K.; Assargren, C.; Gedde, U. W. Polym Test 1990, 9, 241.
67. Lu, X.; Qian, R.; Brown, N. J Mater Sci 1991, 26, 881.
68. Kuhlman, C. J.; Tweedy, L. K.; Kanninen, M. F. Proc Plast Pipes 1992, 8, C2/3-1.
69. Friedrich, K. In Advances in Polymer Science; Kausch, H., Ed.; Springer-Verlag: Berlin, Germany, 1983; Vols. 52 and 53.
70. Kinloch, A. J.; Young, R. J. Fracture Behaviour of Polymers; Applied Science: Barking, England, 1983.
71. Michler, G. H. Kunststoff-Mikromechanik; Hanser: Munich, 1992.
72. Vadimsky, R. G.; Keith, H. D.; Padden, F. J., Jr. J Polym Sci Part A-2: Polym Phys 1969, 7, 1367.
73. Lang, R. W. Ph.D. Thesis, Lehigh University, 1984.